Extreme Mechanics Letters 25 (2018) 53–59

Contents lists available at ScienceDirect

Extreme Mechanics Letters

journal homepage: www.elsevier.com/locate/eml

Magnetic-responsive Fe_3O_4 nanoparticle-impregnated cellulose paper actuators

Xin Wang [a,b], Bin Han [c,d,*], Run-Pei Yu [a,b], Fei-Chen Li [a,b], Zhen-Yu Zhao [a,b], Qian-Cheng Zhang [a,e], Tian Jian Lu [b,e,*]

[a] State Key Laboratory for Strength and Vibration of Mechanical Structures , Xi'an Jiaotong University, Xi'an 710049, China
[b] State Key Laboratory of Mechanics and Control of Mechanical Structures, Nanjing University of Aeronautics and Astronautics, Nanjing 210016, China
[c] School of Mechanical Engineering, Xi'an Jiaotong University, Xi'an 710049, China
[d] School of Engineering, Brown University, Providence, RI 02912, USA
[e] MOE Key Laboratory for Multifunctional Materials and Structures, Xi'an Jiaotong University, Xi'an 710049, China

HIGHLIGHTS

- A type of magnetic-responsive Fe_3O_4 /paper nanocomposite is prepared through a low-cost blending method.
- A reversible and stable performance of flexural actuation of the beam-shaped actuator is achieved due to low magnetic hysteresis loop of the Fe_3O_4 /paper nanocomposite.
- The accordion-shaped actuator can reach a maximum strain of 100% while the star-shaped actuator can capture a spitball twice heavier than itself.

ARTICLE INFO

Article history:
Received 17 July 2018
Received in revised form 10 October 2018
Accepted 11 October 2018
Available online 17 October 2018

Keywords:
Actuator
Cellulose paper
Nanocomposites
Fe_3O_4 nanoparticles
Magnetic hysteresis
Microstructure

ABSTRACT

Fe_3O_4 nanoparticle-infiltrated chromatography paper is prepared using a low-cost blending method. Upon characterizing the basic material properties of the Fe_3O_4/paper nanocomposite, beam-, accordion- and star-shaped actuators are constructed using the nanocomposite and the corresponding actuation performance is investigated experimentally. The beam-shaped actuator exhibits a reversible flexural deformation due to low magnetic hysteresis loop of the Fe_3O_4/paper nanocomposite, maintaining a stable response after 100 cycles. The accordion-shaped actuator can reach a maximum strain of 100% while the star-shaped actuator can capture a spitball twice heavier than itself.

1. Introduction

Cellulose is the most abundant bio-polymer on Earth with low expense, light weight, high availability, good renewability and easy processability [1], has attractive mechanical properties with specific modulus of 100 GPa $cm^3\ g^{-1}$ and specific strength of 4 GPa $cm^3\ g^{-1}$, even higher than that of most metals and composites [2]. Based on the above advantages, cellulose-based materials (wood, hemp, cotton, linen, *etc.*) and their artificial products (paper, textiles, *etc.*) have been widely used for thousand years, almost covering all fields of daily life. Recently, in order to further exploit the mechanical properties, functionality and durability, a lot of novel cellulose-based materials and applications have been proposed in fields, *e.g.*, structural materials [2–4]. energy storage [5–7], flexible electronics [8–10], and sensors [11–13], *etc.* For example, Song et al.[3] created a so-called "super wood" with tensile strength of 587 MPa and specific tensile strength of 451 MPa $cm^3\ g^{-1}$, both of which were even higher than that of metals and alloys. Encouragingly, the corresponding fabrication method is universally effective for various species of wood and deeply inspires the future design of structural materials. Chen et al. proposed a novel design concept of an all-wood-structured, low tortuosity, safe and biodegradable supercapacitor, which is expected to achieve green and renewable energy storage. Liu et al. [9] presented a comprehensive review of paper-based wearable electronics, discussed both pros and cons of each manufacturing tactic, and finally pointed out developing trends of paper-based electronics in the emerging wearable applications.

Cellulose paper, as an artificial product comprising of bio-origin ingredients, is also a common source of cellulose with rich abundance. While cellulose paper is commonly used for printing, packaging, and absorbing liquid, it is attracting remarkably increasing

* Corresponding authors.
E-mail addresses: hanbinghost@mail.xjtu.edu.cn (B. Han), tjlu@nuaa.edu.cn (T.J. Lu).

https://doi.org/10.1016/j.eml.2018.10.003
2352-4316/

research interests for prototyping flexible actuators due to its superiorities including flyweight, mature manufacturing process, favorable mechanical bendability, biocompatibility and nontoxicity over their counterparts. With the development of paper-based devices (low-cost diagnostics [14], scaffolds for cell growth [15], printed electronics [12], flexible sensors [11], *etc.*), it is of great significance to create an actuator, which is embedded within the paper, can be fabricated through a simple method and further operate together with paper-based devices [16]. If mechanical work could be performed with paper-based actuators, novel paper-based machines could be built [17].

More recently, the paper-based actuators can be mainly divided into two categories: single-responsive type and multi-responsive type. As for single-responsive type, the actuators are stimulated by only single external stimulus, such as electricity, humidity, heat or light. Kim et al. [18] firstly proposed an electroactive paper (EAPap) to construct a bending actuator based on the piezoelectric effect of cellulose and ionic transport. Chen et al. [19] developed a paper-based electrostatic zipper actuator consisting of two paper sheets which were printed with the carbon nanotube ink and separated by a dielectric layer (mylar or parylene), and applied the actuating mechanism to the assembly of soft robots. Hamedi et al. [17] created an electrically activated paper-based actuator based on the hygroexpansive property of cellulose papers. For multi-responsive type, Weng et al. [20] fabricated a multi-stimuli responsive actuator via a pencil-on-paper method and achieved bidirectional bending by electricity, humidity and light. However, there are limit research work focusing on designing the magnetic paper actuators. By contrast, magnetic actuators made of hydrogel [21] and polymer [22] have been reported. Herein, inspired by the fabrication method of magnetic hydrogel [21], we proposes a single-magnetic-responsive actuator made of Fe_3O_4 nanoparticle-infiltrated paper that is prepared using a low-cost blending method. The microstructure, phase structure, magnetic properties and mechanical properties of the Fe_3O_4/paper nanocomposite are characterized first. Beam-, accordion- and star-shaped actuators are then designed and the actuation performance is tested.

2. Materials and methods

Whatman chromatography paper Grade A with a thickness of 180 μm and grammage of 88 g/m^2 and Fe_3O_4 nanoparticles with a purity of 99.9% (Sigma-Aldrich Chemicals, USA) are chosen as basic materials to construct the Fe_3O_4/paper nanocomposite. The average particle size, density and specific surface area of the Fe_3O_4 nanoparticles are 20 nm, 5.18 g/cm^3 and 50 m^2/g, respectively. Tetramethyl Ammonium Hydroxide (Aladdin Chemicals, China) is used as the surfactant. Tributyl Phosphate (Guangzhou Jinhuada, China) is employed to reduce bubbles generated during stirring.

Before fabricating the Fe_3O_4/paper nanocomposite, 25wt% Fe_3O_4 nanofluid is prepared by dispersing Fe_3O_4 nanoparticles into deionized water based on the method used in Ref. [23]. The Fe_3O_4 nanoparticles can easily agglomerate and sedimentate, attributed to their high specific surface area and surface activity. As the surfactant, Tetramethyl Ammonium Hydroxide is subsequently added into the nanofluid, with a mass proportion of 1:3 relative to the nanoparticles. The mixture is then mechanically stirred for 1 h with a rate of 2000 rmp (motor stirrer, JJ-1H), followed immediately by ultrasonic waves treatment at 20 kHz for 0.5 h (ultrasonic cleaning machine, BRANSON 1800). To minimize bubbles generated during stirring, Tributyl Phosphate with a bulk volume of 1–2 ml is added into the mixture.

Fig. 1 shows the fabrication process of Fe_3O_4/paper nanocomposite: (1) Fe_3O_4 nanofluid with a pipette is added to the paper sheet until full saturation; (2) the impregnated paper sheet is dried; (3) the dried paper sheet is stored in a chamber of constant temperature and humidity. Note that, the impregnated paper sheet is dehydrated on an electric heating plate at 70 °C for 10 min, and subsequently preserved at fixed temperature (23 °C) and relative humidity (50%).

The microstructure of as-fabricated nanocomposite (surface and cross section) is analyzed using scanning electron microscopy (SEM, Hitachi S-3000N) and energy dispersive X-ray spectroscopy (EDS, Oxford X-act). SEM images are taken at a working distance of 14.9 mm with a voltage of 15 kV and a probe current of 109 μA, while EDS measurements are made with a voltage of 20 kV and a probe current of 144 μA. The phase structure of pure Fe_3O_4 nanoparticles and Fe_3O_4/paper nanocomposite is observed using X-ray diffraction (XRD, X'Pert PROMPP). The magnetic properties (i.e., magnetic hysteresis loop, saturation magnetization, remnant field and coercive field) of pure Fe_3O_4 nanoparticles and Fe_3O_4/paper nanocomposite at ambient temperature are investigated using a vibrating-sample magnetometer (VSM, Lakershore 7404) with a maximum applied field of 2.17 T. Tensile tests of Fe_3O_4/paper nanocomposites are carried out using a universal testing machine (SHIMAZU, AG-Xplus). The load cell for tension has a maximum capacity of 1000 N, minimum force resolution of 0.83 N, and minimum displacement resolution of 0.033 μm. According to ASTM Standard D882, the tensile specimens are cut into strips with the length of 150 mm, width of 10 mm and gauge length of 100 mm. The thickness of the specimens is measured using a digital micrometer (NSCING, Nanjing) with resolution of 0.001 mm.

3. Results and discussions

The amount of Fe_3O_4 nanoparticles embedded into the paper-based nanocomposites was measured and it was associated with the porosity of paper material and the concentration of Fe_3O_4 nanofluid [24]. The mass percentage of Fe_3O_4 nanoparticles in the present nanocomposite is measured as 46.80%±1.88%, the thickness of the composite film is around 193 μm, and the corresponding density is 0.857 g/cm^3. Fig. 2a-d show the surface microstructure of the nanocomposite. It is observed from SEM images (Fig. 2a-c) that Fe_3O_4 nanoparticles are diffused into the porous regions among cellulose fiber networks. It is found from the EDS map (Fig. 2d, blue points represent Fe element) that Fe_3O_4 nanoparticles are uniformly distributed on the surface of cellulose fibers. Besides, the cross-section morphology of the nanocomposite is also observed through SEM and EDS images, as shown in Fig. 3a-d. To analyze the diffusion of Fe_3O_4 nanoparticles through thickness direction, EDS images of Fe element on the cross section (Fig. 3d, blue points represent Fe element) are measured. It is found that Fe element of the current nanocomposite is uniformly distributed through thickness direction.

XRD patterns of both pure Fe_3O_4 nanoparticles and Fe_3O_4/paper nanocomposite are shown in Fig. 4a-b. Fig. 4a shows that Fe_3O_4 is the major phase in the pure nanoparticles, which is similar to the prior experimental results in Ref. [25]. By contrast, the major phases of the nanocomposite are Fe_3O_4 and cellulose (the first major peak in Fig. 4b). Although the intensity of the nanocomposite is lower than that of the pure nanoparticles, the major phase of Fe element is not changed. Fig. 4c displays the magnetic hysteresis loops of both pure Fe_3O_4 nanoparticles and Fe_3O_4/paper nanocomposite at ambient temperature (25 °C). Under an external magnetic field, the magnetic moment of Fe_3O_4 nanoparticles is exerted along the magnetic gradient direction, and the magnetization increases with magnetic field until saturation [26]. The pure Fe_3O_4 nanoparticles show a saturation magnetization of 63.1 emu/g, a remnant field of 3.4 emu/g and a coercive field of 35.3 Oe. As for the Fe_3O_4/paper nanocomposite, the saturation magnetization, remnant field, and coercive field are 33.5 emu/g, 2.2 emu/g and 28.7 Oe, respectively. The Young's modulus, tensile strength, toughness and fracture

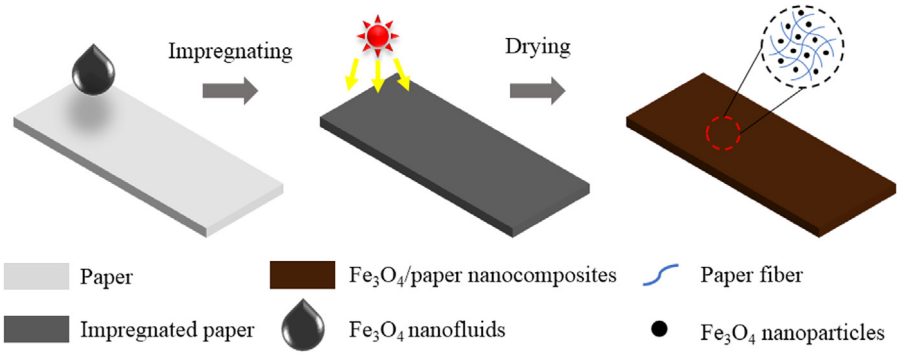

Fig. 1. Fabrication process of Fe_3O_4/paper nanocomposite via a low-cost blending method.

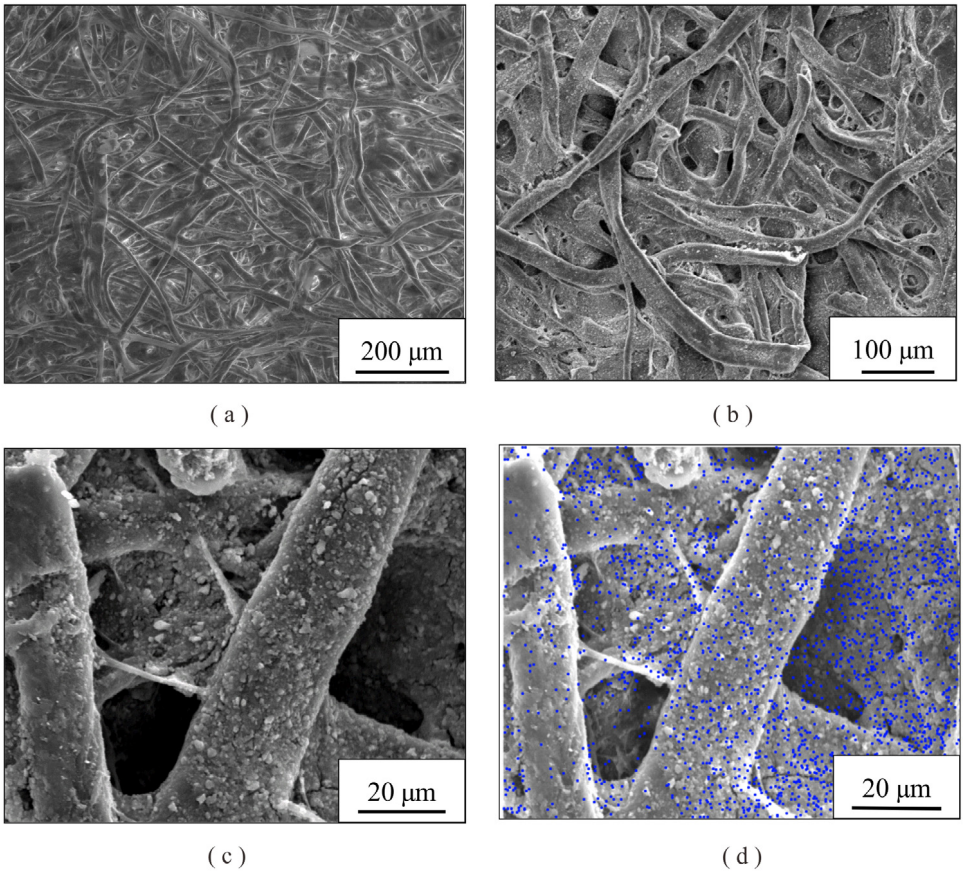

Fig. 2. Surface morphology of Fe_3O_4/paper nanocomposite. (a), (b) and (c) SEM images of Fe_3O_4/paper nanocomposite; (d) EDS image of Fe_3O_4/paper nanocomposite (blue points represent Fe elements). (For interpretation of the references to color in this figure legend, the reader is referred to the web version of this article.)

Table 1
Mechanical properties of Fe_3O_4/paper nanocomposite.

Direction	Young's modulus (MPa)	Tensile strength (MPa)	Toughness (MJ/m^3)	Fracture strain (%)
MD	769.1 ± 24.3	4.94 ± 0.31	0.062 ± 0.004	1.74 ± 0.08
CD	504.8 ± 29.7	3.45 ± 0.28	0.061 ± 0.007	2.42 ± 0.05

strain of Fe_3O_4/paper nanocomposite are measured via tensile testing, as shown in Table 1 and Fig. 4d. On account of the highly anisotropic behaviors of chromatography paper [27], the specimens are tailored along both the machine direction (MD) and the cross-machine direction (CD). The nanocomposite has better mechanical properties along MD than those along CD. Hence, the magnetic paper-based actuators are fabricated using the Fe_3O_4/paper nanocomposite along MD.

The force F_m exerted on each Fe_3O_4 nanoparticle points along the maximum magnetic gradient direction is given by [28]

$$F_m = \frac{\chi_p V_p}{\mu_0} B(\nabla B) \tag{1}$$

where μ_0 is the permeability of free space ($4\pi \times 10^{-7}$ H/m), χ_p is the susceptibility of nanoparticles, V_p is the volume of a nanoparticle, B and ∇B are the magnetic flux density and magnetic field gradient, respectively. Thus, under a tunable magnetic field,

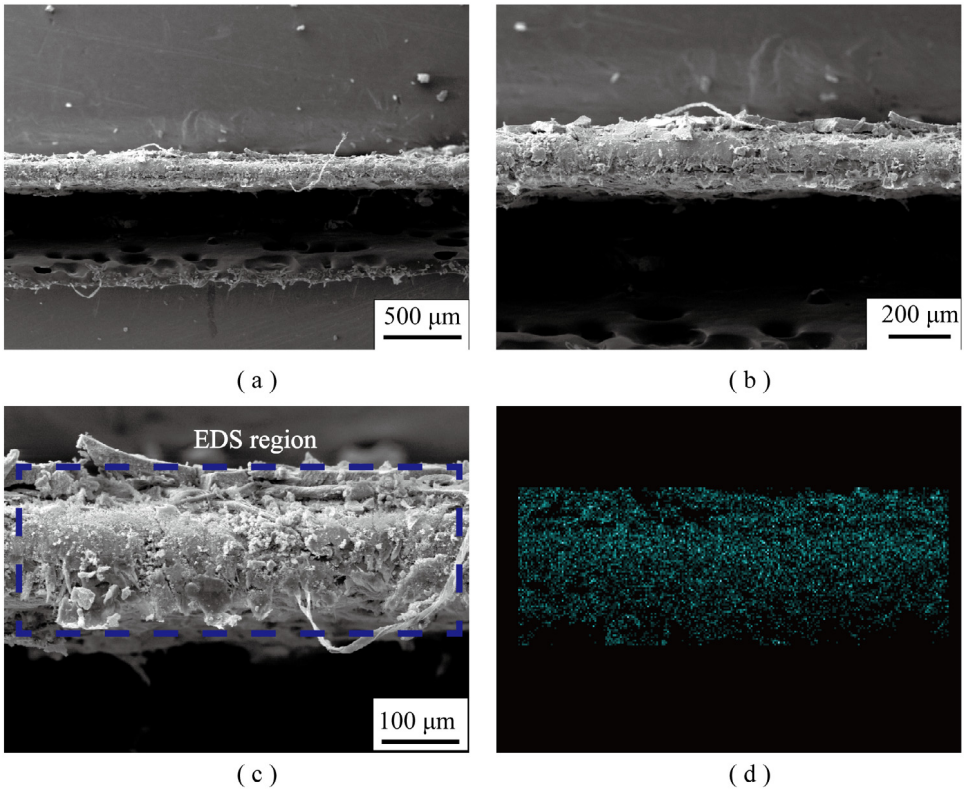

Fig. 3. Cross section morphology of Fe_3O_4/paper nanocomposite. (a), (b) and (c) SEM images of Fe_3O_4/paper nanocomposite (blue frame line represent EDS region); (d) EDS image of Fe_3O_4/paper nanocomposite (blue points represent Fe elements). (For interpretation of the references to color in this figure legend, the reader is referred to the web version of this article.)

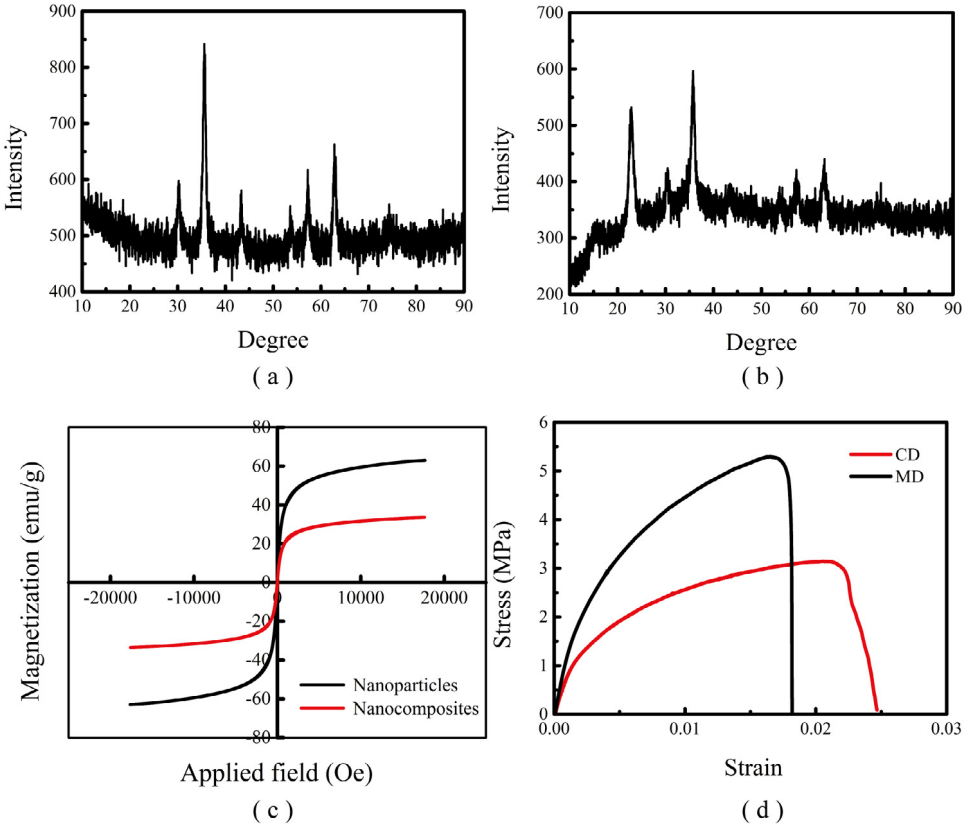

Fig. 4. XRD patterns of (a) pure Fe_3O_4 nanoparticles and (b) Fe_3O_4/paper nanocomposites; (c) Magnetic hysteresis loop of pure Fe_3O_4 nanoparticles and Fe_3O_4/paper nanocomposites; (d) Typical tensile stress–strain curves of Fe_3O_4/paper nanocomposites along MD and CD, respectively.

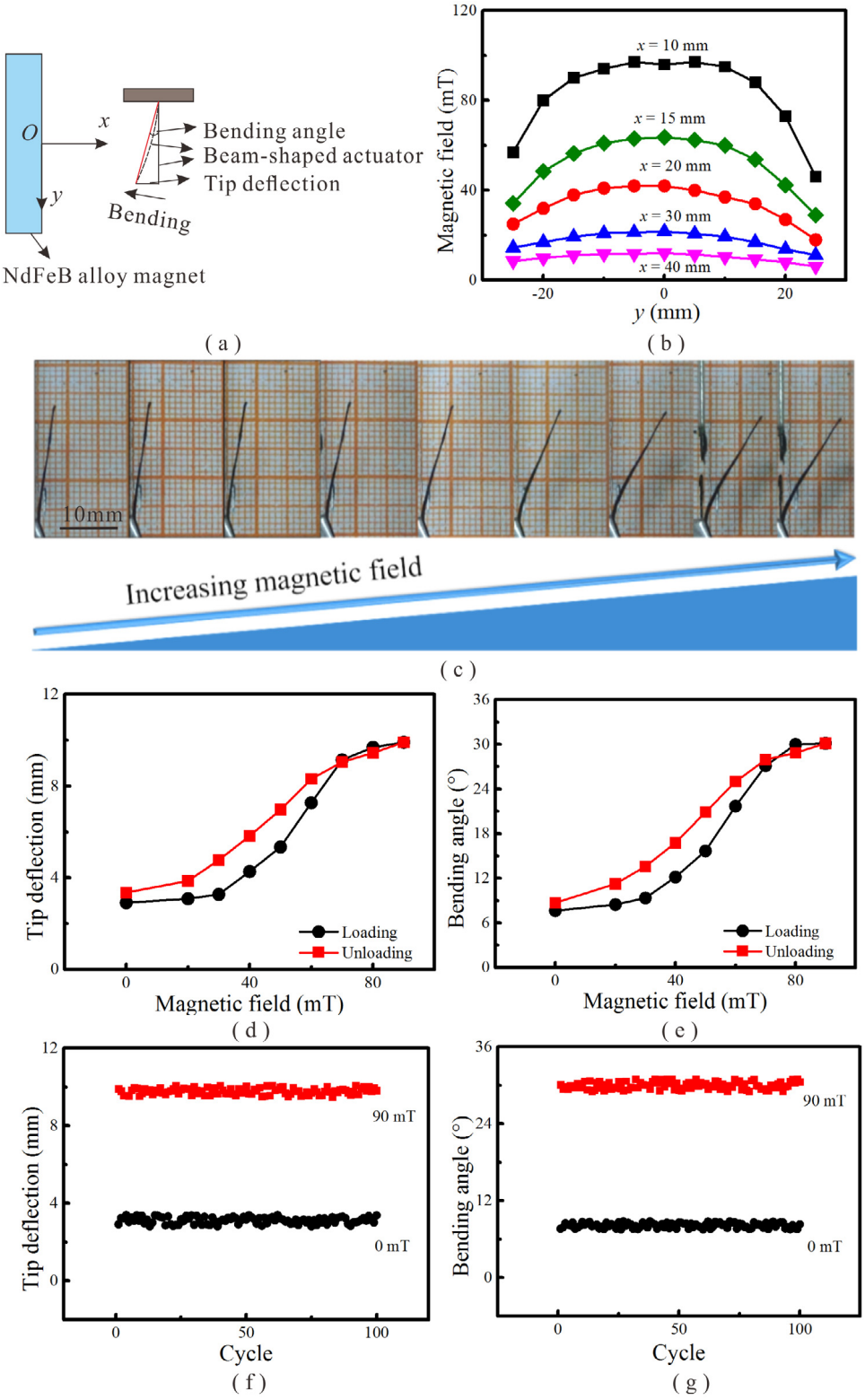

Fig. 5. Performance of beam-shaped Fe_3O_4/paper actuator under tunable magnetic field: (a) Experimental principle; (b) Distribution of magnetic field; (c) Photographs of actuator responses with increased magnetic field; (d) tip deflection and (e) bending angle as functions of magnetic field; (f) and (g) Repeatability test results with magnetic field varying periodically between 0 mT and 90 mT.

Fe_3O_4 nanoparticles can drive the Fe_3O_4/paper composite to work as an actuator.

Based upon the Fe_3O_4/paper nanocomposite, three types of actuator are designed with their actuation performance measured. Fig. 5a presents a beam-shaped actuator with in-plane dimensions of 20 mm ×2 mm, which is attached on a polymethyl methacrylate block with one end clamped by adhesive tape. With a tunable external magnetic field produced by adjusting the distance between the actuator and a permanent NdFeB alloy magnet, the tip deflection and bending angle at the free end are measured. The

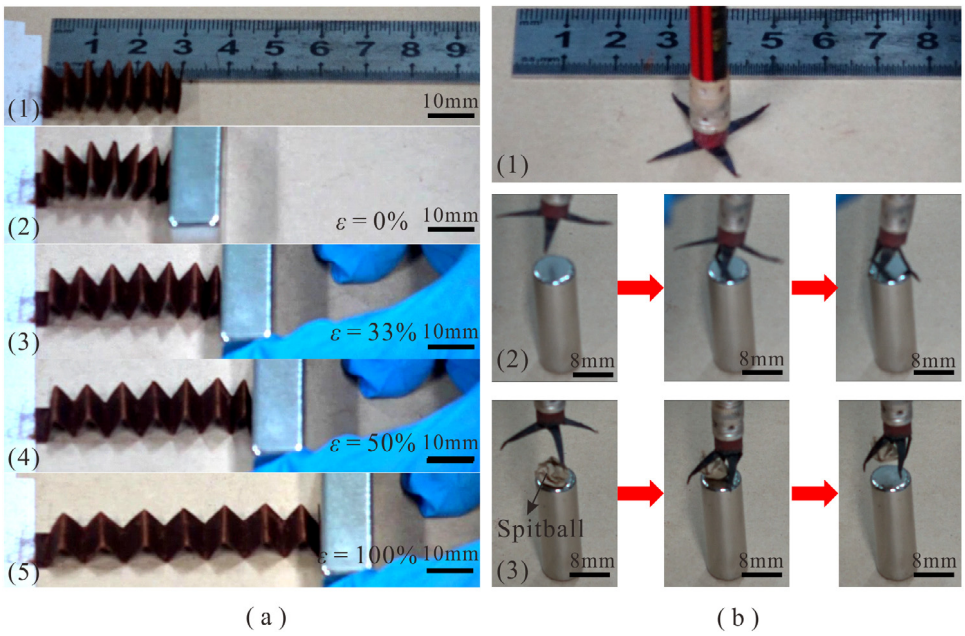

Fig. 6. (a) Performance of accordion-shaped Fe_3O_4/paper actuator subjected to tunable magnetic field. (1–5) show actuator deformation magnetically actuated at specific normal strains. (b) Performance of star-shaped Fe_3O_4/paper actuator under tunable magnetic field: (1) Initial condition of actuator; (2) Snapshots of gripping process; (3) Snapshots of capturing process.

distribution of the magnetic field measured using Gauss meter is presented in Fig. 5b. The magnetic intensity decreases as the distance between the magnet and the actuator is increased, while loading and unloading (hysteresis test) are achieved by placing and removing the magnet. Fig. 5c shows a snapshot of the beam-shaped actuator driven by an increasing magnetic intensity. Due to fabrication defects and self-weight, the actuator has an initial tip deflection of 2.91 mm and bending angle of 7.63°. Both the tip deflection and bending angle increase with increasing magnetic field, peaking at 9.91 mm and 30.12° when the magnetic field reaches 90 mT. Subsequently, as the magnetic field is gradually reduced to 0 mT, the tip deflection and bending angle recover to 3.35 mm and 8.7°, close to the initial values. This small hysteresis effect is likely attributed to the large bending deformation which may exceed the elastic deformation of the nanocomposite, causing irreversible deformation. Fig. 5f-g presents the repeatability as the magnetic field is varied periodically between 0 mT and 90 mT. The actuation performance remains stable even after 100 cycles of loading and unloading, existing good robustness. Compared to the prior magnetic actuator [24], the as-fabricated actuator exhibits a reversible flexural deformation due to low magnetic hysteresis loop of the Fe_3O_4/paper nanocomposite, reduces the fabrication expense and facilitates the further applications.

As the Fe_3O_4/paper nanocomposite is mechanical foldable, an accordion-shaped actuator with prefolded creases is fabricated, as shown in Fig. 6a. To this end, the Fe_3O_4/paper strip with a length of 100 mm and width of 10 mm is folded 13 times. The actuator is actuated by a NdFeB magnet with the magnetic intensity of about 230 mT. During the experiment, the maximum deformation and strain achieved by the accordion-shaped actuator are 30 mm and 100%, respectively. Inspired by the Venus flytrap which could close their leaves within a second for efficient prey capture [29], a star-shaped actuator is proposed as a paper-based biomimetic gripper which is fabricated based on the Fe_3O_4/paper nanocomposite, as shown in Fig. 6b. Under a magnetic field, it behaves as a gripper and can capture and lift a spitball almost twice as heavy as the actuator.

4. Conclusions

Cellulose paper material and Fe_3O_4 nanoparticles are used to fabricate Fe_3O_4/paper nanocomposite using a low-cost blending method. The nanocomposite is then used to construct novel paper-based magnetic actuators having different shapes. When subjected to an external magnetic field, the paper-based actuators display large deformation, high stability and reversible response. The beam-shaped actuator achieves a nearly reversible and robust bending response, the accordion-shaped actuator reaches a maximum strain of 100%, while the star-shaped actuator captures a spitball twice heavier than itself. The proposed magnetic-responsive paper actuators hold great potential in the fields of artificial muscles, soft robots, origami-inspired devices, magnetic self-assembly and lab-on-paper devices.

Acknowledgments

This work was supported by the National Natural Science Foundation of China (11802221, and 11472208), the National Key R&D Program of China (2018YFB1106400), China Postdoctoral Science Foundation (2016M600782), Zhejiang Provincial Natural Science Foundation of China (LGG18A020001), Postdoctoral Scientific Research Project of Shaanxi Province (2016BSHYDZZ18), Natural Science Basic Research Plan in Shaanxi Province of China (2018JQ1078).

References

[1] R.J. Moon, A. Martini, J. Nairn, J. Simonsen, J. Youngblood, Cellulose nanomaterials review: structure, properties and nanocomposites, Chem. Soc. Rev. 40 (2011) 3941–3994.
[2] H. Zhu, S. Zhu, Z. Jia, S. Parvinian, Y. Li, O. Vaaland, L. Hu, T. Li, Anomalous scaling law of strength and toughness of cellulose nanopaper, Proc. Natl. Acad. Sci. 112 (2015) 8971–8976.
[3] J. Song, C. Chen, S. Zhu, M. Zhu, J. Dai, U. Ray, Y. Li, Y. Kuang, Y. Li, N. Quispe, Y. Yao, A. Gong, U.H. Leiste, H.A. Bruck, J.Y. Zhu, A. Vellore, H. Li, M.L. Minus, Z. Jia, A. Martini, T. Li, L. Hu, Processing bulk natural wood into a high-performance structural material, Nature 554 (2018) 224–228.
[4] Y. Li, H. Zhu, S. Zhu, J. Wan, Z. Liu, O. Vaaland, S. Lacey, Z. Fang, H. Dai, T. Li, L. Hu, Hybridizing wood cellulose and graphene oxide toward high-performance fibers, NPG. Asia. Mater. 7 (2015) 150.

[5] D. Xu, C. Chen, J. Xie, B. Zhang, L. Miao, J. Cai, Y. Huang, L. Zhang, A hierarchical N/S-codoped carbon anode fabricated facilely from cellulose/polyaniline microspheres for high-performance sodium-ion batteries, Adv. Energ. Mater. 6 (2016) 150192.
[6] C. Chen, Y. Zhang, Y. Li, J. Dai, J. Song, Y. Yao, Y. Gong, I. Kierzewski, J. Xie, L. Hu. All-wood, low. tortuosity, aqueous, low tortuosity aqueous biodegradable supercapacitors with ultra-high capacitance, Energy Environ. Sci. 10 (2017) 538–545.
[7] V.L. Pushparaj, M.M. Shaijumon, A. Kumar, S. Murugesan, L. Ci, R. Vajtai, R.J. Linhardt, O. Nalamasu, P.M. Ajayan, Flexible energy storage devices based on nanocomposite paper, Proc. Natl. Acad. Sci. 104 (2007) 13574–13577.
[8] D. Tobjork, R. Osterbacka, Paper electronics, Adv. Mater. 23 (2011) 1935–1961.
[9] H. Liu, H. Qing, Z. Li, Y.L. Han, M. Lin, H. Yang, A. Li, T.J. Lu, F. Li, F. Xu, Paper: A promising material for human-friendly functional wearable electronics, Mater. Sci. Eng. 112 (2017) 1–22.
[10] M.M. Hamedi, A. Ainla, F. Guder, D.C. Christodouleas, M.T. Fernandez-Abedul, G.M. Whitesides, Integrating electronics and microfluidics on paper, Adv. Mater. 28 (2016) 5054–5063.
[11] T. Dinh, H.P. Phan, T.K. Nguyen, A. Qamar, P. Woodfield, Y. Zhu, N.T. Nguyen, D. Viet Dao, Solvent-free fabrication of biodegradable hot-film flow sensor for noninvasive respiratory monitoring, J. Phys. D: Appl. Phys. 50 (2017) 215401.
[12] N. Ruecha, O. Chailapakul, K. Suzuki, D. Citterio, Fully inkjet-printed paper-based potentiometric ion-sensing devices, Anal. Chem. 89 (2017) 10608–10616.
[13] C.W. Lin, Z. Zhao, J. Kim, J. Huang, Pencil drawn strain gauges and chemiresistors on paper, Sci. Rep. 4 (2014) 3812.
[14] J. Hu, S. Wang, L. Wang, F. Li, B.P. Murphy, T.J. Lu, F. Xu, Advances in paper-based point-of-care diagnostics, Biosens. Bioelectron. 54 (2014) 585–597.
[15] R. Derda, A. Laromaine, A. Mammoto, S.K. Tang, T. Mammoto, D.E. Ingber, G.M. Whitesides, Paper-supported 3d cell culture for tissue-based bioassays, Proc. Natl. Acad. Sci. 106 (2009) 18457–18462.
[16] M. Weng, P. Zhou, L. Chen, L. Zhang, W. Zhang, Z. Huang, C. Liu, S. Fan, Multiresponsive bidirectional bending actuators fabricated by a pencil-on-paper method, Adv. Funct. Mater. 26 (2016) 7244–7253.
[17] M.M. Hamedi, V.E. Campbell, P. Rothemund, F. Güder, D.C. Christodouleas, J.F. Bloch, G.M. Whitesides, Electrically activated paper actuators, Adv. Funct. Mater. 26 (2016) 2446–2453.
[18] J. Kim, S. Yun, Z. Ounaies, Discovery of cellulose as a smart material, Macromolecules 39 (2006) 4202–4206.
[19] A.S. Chen, H. Zhu, Y. Li, L. Hu, A paper-based electrostatic zipper actuator for printable robots, in: IEEE ICRA, 2014, pp. 5038–5043.
[20] M. Weng, P. Zhou, L. Chen, L. Zhang, W. Zhang, Z. Huang, C. Liu, S. Fan, Multiresponsive bidirectional bending actuators fabricated by a pencil-on-paper method, Adv. Funct. Mater. 26 (2016) 7244–7253.
[21] H. Haider, C.H. Yang, W.J. Zheng, J.H. Yang, M.X. Wang, S. Yang, M. Zrinyi, Y. Osada, Z. Suo, Q. Zhang, J. Zhou, Y.M. Chen, Exceptionally tough and notch-insensitive magnetic hydrogels, Soft. Matter. 11 (2015) 8253–8261.
[22] M.M. Said, J. Yunas, R.E. Pawinanto, B.Y. Majlis, B. Bais, PDMS based electromagnetic actuator membrane with embedded magnetic particles in polymer composite, Sensors Actuators A 245 (2016) 85–96.
[23] L. Sha, Y. Ju, H. Zhang, J. Wang, Experimental investigation on the convective heat transfer of Fe3O4/water nanofluids under constant magnetic field, Appl. Therm. Eng. 113 (2017) 566–574.
[24] Z. Ding, P. Wei, G. Chitnis, B. Ziaie, Ferrofluid-impregnated paper actuators, J. Microelectromech. S. 20 (2011) 59–64.
[25] A.C. Small, J.H. Johnston, Novel hybrid materials of magnetic nanoparticles and cellulose fibers, J. Colloid. Interf. Sci. 331 (2009) 122.
[26] J. Guo, H.B. Gu, H.G. Wei, Q.Y. Zhang, N. Haldolaarachchige, Y. Li, D.P. Young, S.Y. Wei, Z.H. Guo, Magnetite-polypyrrole metacomposites: dielectric properties and magnetoresistance behavior, J. Phys. Chem. C. 117 (2013) 10191–10202.
[27] Q.S. Xia, M.C. Boyce, D.M. Parks, A constitutive model for the anisotropic elastic–plastic deformation of paper and paperboard, Int. J. Solids Struct. 39 (2002) 4053–4071.
[28] K. Zhang, Q. Liang, S. Ma, X. Mu, P. Hu, Y. Wang, G. Luo, On-chip manipulation of continuous picoliter-volume superparamagnetic droplets using a magnetic force, Lab. Chip. 9 (2009) 2992–2999.
[29] Y. Forterre, J.M. Skotheim, J. Dumais, L. Mahadevan, How the venus flytrap snaps, Nature 433 (2005) 421.